

Research of influence of the additional electrode on Hall thruster plume by particle-in-cell simulation

Xi-Feng Cao(曹希峰), Hui Liu(刘辉), Da-Ren Yu(于达仁)

Citation: Chin. Phys. B . 2020, 29(9): 095204 . **doi:** 10.1088/1674-1056/aba2e3
Journal homepage: http://cpb.iphy.ac.cn; http://iopscience.iop.org/cpb

What follows is a list of articles you may be interested in

The *E*×*B* drift instability in Hall thruster using 1D PIC/MCC simulation

Zahra Asadi, Mehdi Sharifian, Mojtaba Hashemzadeh, Mahmood Borhani Zarandi, Hamidreza Ghomi Marzdashti

Chin. Phys. B . 2020, 29(2): 025204 . **doi:** 10.1088/1674-1056/ab6719

Experimental and numerical investigation of a Hall thruster with a chamfered channel wall

Hong Li(李鸿), Guo-Jun Xia(夏国俊), Wei Mao(毛威), Jin-Wen Liu(刘金文), Yong-Jie Ding(丁永杰), Da-Ren Yu(于达仁), Xiao-Gang Wang(王晓钢)

Chin. Phys. B . 2018, 27(10): 105209 . **doi:** 10.1088/1674-1056/27/10/105209

Influence of channel length on discharge performance of anode layer Hall thruster studied by particle-in-cell simulation

Xi-Feng Cao(曹希峰), Hui Liu(刘辉), Wen-Jia Jiang(蒋文嘉), Zhong-Xi Ning(宁中喜), Run Li(黎润), Da-Ren Yu(于达仁)

Chin. Phys. B . 2018, 27(8): 085204 . **doi:** 10.1088/1674-1056/27/8/085204

Particle-in-cell simulation for the effect of magnetic cusp on discharge characteristics in a cylindrical Hall thruster

Sheng-Tao Liang(梁圣涛), Hui Liu(刘辉), Da-Ren Yu(于达仁)

Chin. Phys. B . 2018, 27(4): 045201 . **doi:** 10.1088/1674-1056/27/4/045201

Low-frequency oscillations in Hall thrusters

Wei Li-Qiu, Han Liang, Yu Da-Ren, Guo Ning

Chin. Phys. B . 2015, 24(5): 055201 . **doi:** 10.1088/1674-1056/24/5/055201

Research of influence of the additional electrode on Hall thruster plume by particle-in-cell simulation*

Xi-Feng Cao(曹希峰), Hui Liu(刘辉)†, and Da-Ren Yu(于达仁)‡

Laboratory of Plasma Propulsion, Harbin Institute of Technology, Harbin 150001, *China*

(Received 17 May 2020; revised manuscript received 29 June 2020; accepted manuscript online 6 July 2020)

Hall thruster is an electric propulsion device for attitude control and position maintenance of satellites. The discharge process of Hall thruster will produce divergent plume. The plume will cause erosion, static electricity, and other interference to the main components, such as solar sailboard, satellite body, and thruster. Therefore, reducing the divergence of the plume is an important content in the research of thruster plume. The additional electrode to the plume area is a way to reduce the divergence angle of the plume, but there are few related studies. This paper uses the particle-in-cell (PIC) simulation method to simulate the effect of the additional electrode on the discharge of the Hall thruster, and further explains the effect mechanism of the additional electrode on parameters such as the electric field and plume divergence angle. The simulation results show that the existence of the additional electrode can enhance the potential near the additional position. The increase of the potential can effectively suppress the radial diffusion of ions, and effectively reduce the plume divergence angle. The simulation results show that when the additional electrode is 30 V, the half plume divergence angle can be reduced by 18.21%. However, the existence of additional electric electrode can also enhance the ion bombardment on the magnetic pole. The additional electrode is relatively outside, the plume divergence angle is relatively small, and it can avoid excessive ion bombardment on the magnetic pole. The research work of this paper can provide a reference for the beam design of Hall thruster.

Keywords: Hall thruster, additional electrode, plume divergence

PACS: 52.75.Di, 52.65.–y, 52.65.Pp, 52.65.Rr **DOI:** 10.1088/1674-1056/aba2e3

1. Introduction

The Hall thruster is an electric propulsion device, which has been widely used in satellite location maintenance, attitude adjustment, orbit change, resistance compensation, and many interplanetary missions.[1–5] The principle of Hall thruster is to use an orthogonal electromagnetic field to ionize the propellant gas and accelerate the ions to generate thrust. As the propellant gas, xenon and krypton are generally used. The structure of Hall thruster is shown in Fig. 1. Due to factors such as the electric field in the radial direction, ions have a radial velocity. Therefore, when the ions enter the plume region, they will diffuse to both sides of the thruster and form the plume divergence angle (which is considered to account for 90% of the total plume). Large plume divergence angle will cause plume pollution, which will have an impact on the satellite body and solar panels and other components.

At present, many scholars have carried out related research work to reduce the plume divergence angle of the Hall thruster, such as using additional electrode[6–10] and optimizing the position of the cathode.[11] These methods can effectively reduce the plume divergence angle. There are two methods to deal with the additional electrode, one is to add an additional electrode inside the channel,[12,13] the other is to add an additional electrode in the plume area.[6,14] The current research mainly focuses on the additional electrode inside the channel, trying to improve the thruster performance by changing the ionization inside the channel, but this method cannot directly and effectively reduce the plume divergence angle. However, there are relatively few studies on the additional electrode in the plume area. In the experiment, Gridwords *et al.* initially tried to add electrodes at different axial positions in the plume area. The experimental results show that the additional electric field can reduce the plume divergence angle.[14] In their experiment, the additional electrode was placed farther away from the thruster, and the potential on the additional electrode was high, which increased the power burden. Therefore, this scheme of additional electrode is not easy to adopt in practical applications. So, in this paper, we adopt a scheme that the additional electrode is close to the thruster and has a low voltage. In order to better study the effect of additional electrode on the micro parameters, the PIC simulation method is used to simulate the discharge process of the Hall thruster under the different additional electrode conditions. And the effects of the additional electrode on the parameters such as potential and plasma density are compared. The effects of additional electrode on macroscopic parameters are

*Project supported by the National Natural Science Foundation of China (Grant No. 51776047), the Key Project of the National Natural Science Foundation of China (Grant No. 51736003), the Civil Aerospace Pre-research Project (Grant No. D010509), and the Open Fund of Beijing Institute of Control Engineering (Grant No. LabASP-2018-13).

†Corresponding author. E-mail: thruster@126.com

‡Corresponding author. E-mail: yudaren@hit.edu.cn

© 2020 Chinese Physical Society and IOP Publishing Ltd

also analyzed such as plume divergence angle and the bombardment effect of ions on the magnetic pole. The rest of this paper is organized as follows: the second part introduces the computational model, and the third part discusses the results and analysis of numerical simulations. Finally, the fourth part is the conclusion.

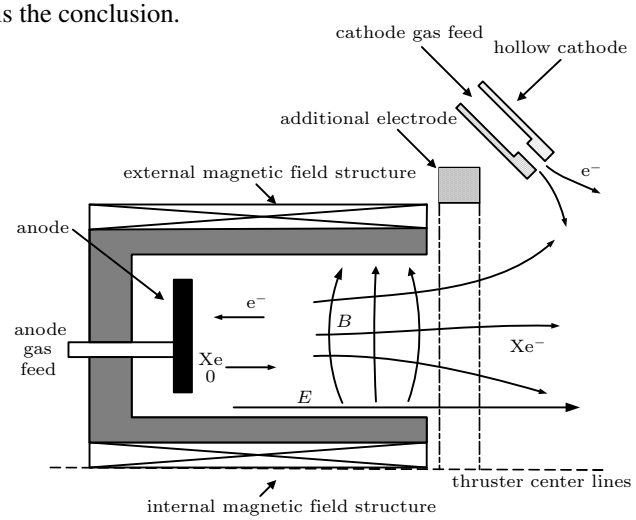


Fig. 1. The structure diagram of Hall thruster.

2. Numerical model

Because the structure of Hall thruster is axisymmetric, we use a two-dimensional simulation in this paper. The simulation area is shown in Fig. 2, including anode, channel, and near-field plume area. We use PIC method to simulate the movement of particles including atoms, electrons, and ions. And we use the Monte Carlo method (MCC) to simulate the collision between particles. The elastic, excitation, and single ionization collisions between electrons and atoms are considered in the model. The electric field is solved by the Poisson equation. The magnetic field generated by the plasma is ignored, because it is much smaller than that generated by coils and permanent magnets. We have used this model to study Hall thruster, multi-cusped field thrusters, and so on.[15–21]

The boundary conditions are shown in Fig. 2, including the anode, dielectric, metal wall, cathode, free boundary, and symmetry boundary. The treatment methods for the different boundary conditions are selected. The potential of anode is 300 V, and the gas flow is 30 sccm. The BN ceramic is used as the channel wall which is insulated. And the secondary electron emission model in literature 22 is used in this paper. The cathode adopts quasi-neutral boundary model. The energy of electrons is 2 eV.[23–25] The metal wall adopts a capacitive charging model.[26] When the particles cross the free boundary, the particles are considered to disappear. And when the particles cross the symmetry boundary, the particles will be reflected.

In this paper, we also consider the condition of the additional electrode, so we set the additional electrode in the upper boundary area of the plume, as shown in Fig. 2. In order to simplify the simulation conditions, we treat the additional electrode as a fixed potential boundary, so we ignore the influence of electrode structure. And in order to investigate the influence of the additional electrode position, we selected two additional electrode positions, $Z = 0.03$ m–0.045 m (as left electrode) and $Z = 0.045$ m–0.06 m (as right electrode), as shown in Fig. 2. This design scheme of the additional electrode position close to the thruster is easier to implement in practical applications, and can effectively reduce the bombardment on the additional electrode by the beam ions. Since in this paper, we mainly study the influence of the additional electrode on the parameter distribution in the plume region. In order to avoid the excessive interference of the additional electrode on the main beam region, we choose a relatively low additional potential value. The additional potential value used in this paper are set to 10 V, 20 V, and 30 V, respectively. When the particles hit the additional electrode, the particles are treated in the same way as under free boundary. For comparison, we also simulate the condition without the additional electrode. This condition is recorded as the condition of initial. We use FEMM software to obtain the magnetic field distribution, as shown in Fig. 2. The peak of the magnetic field is located at the channel outlet.

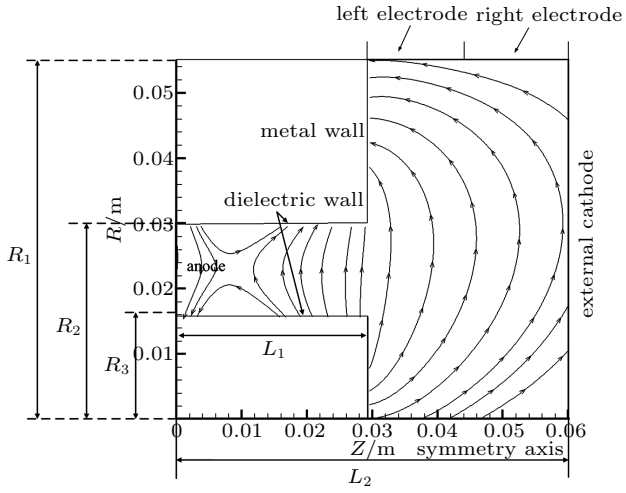


Fig. 2. Computational domain and boundary.

The relevant parameters used in this paper are shown in Table 1.

Table 1. The area parameters in calculations.

Parameter name	Parameter value
Inner channel radius R_1/mm	16
Outer channel radius R_2/mm	29
Channel length L_1/mm	30
Calculated area radius R_3/mm	55
Calculated area length L_3/mm	60
Total radial grid	110
Total axial grid	120
Anode potential/V	300

In this paper, we use the orthogonal grid. The size of the grid length is 0.5 mm, which is about 0.5 times the Debye length. The time step Δt equals a smaller value of $0.1\omega_{pe}^{-1}$ and $0.35\omega_c^{-1}$, where ω_{pe} is the electron oscillation frequency and ω_c is the electron cyclotron frequency. Because the electron oscillation is smaller and the value is about 10^{11} Hz, the time step Δt is taken as 10^{-12} s.

3. Simulation results and analyses

3.1. Potential and density distribution

Firstly, we compare the distribution of potential and ion density, and the distributions of potential and ion density under the seven conditions are similar. Here we only show the two-dimensional distribution of potential and ion density under the condition of initial (no additional electrode), as shown in Figs. 3 and 4. It can be found that the potential decreases gradually from anode to plume, and the potential drop is mainly concentrated in the channel. Comparing the distribution of ion density, it can be found that the ionization region is mainly in the channel.

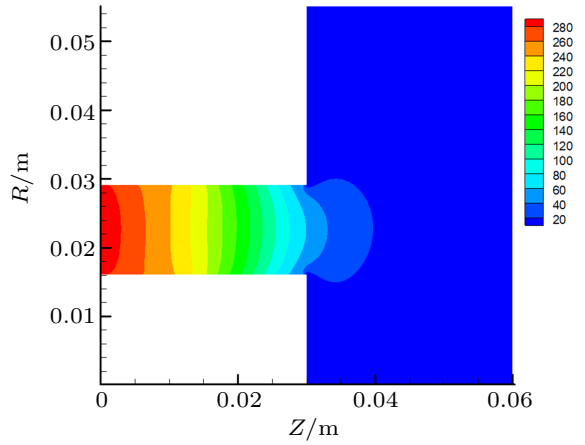


Fig. 3. Two-dimensional distribution of potential (initial case).

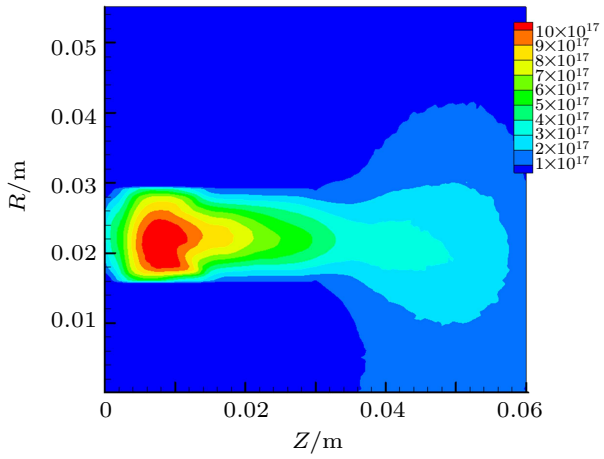


Fig. 4. Two-dimensional distribution of ion number density (initial case).

Further the distribution of potential along the central axis of the channel is compared, as shown in Fig. 5. The comparison results show that the potential distribution along the central axis of the channel changes little, which indicates that the additional electrode has little effect on the potential in the beam region.

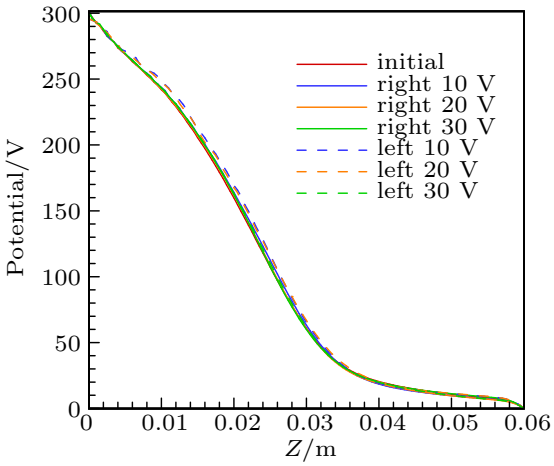


Fig. 5. The distribution of potential along the central axis of the channel.

In order to further compare the effect of the additional electrode on the distribution of potential in the plume region, we made a separate comparison of the potential distribution in the near field plume region, as shown in Fig. 6. And only the simulation results under three conditions are shown in Fig. 6, initial case means the condition without additional electrode, and case-left 30 V and case-right 30 V means that the additional electrodes are on the left side and right side respectively, and the potential is 30 V. Firstly, it can be found that the potential in the near-field plume mainly presents two-dimensional fan-shaped distribution. Near the central axis of the exit, the potential gradually decreases along the magnetic field line to both sides, as shown in Fig. 6(a). Since the magnetic field lines are approximately perpendicular to the central axis of the channel, and the magnetic field lines are significantly curved on both sides of the thruster. Along the magnetic field lines, Ohm's law can be approximated by Boltzmann's law as follows.[27] Where CL represents the channel centerline. n_0 is the plasma density, T_e is the temperature of the plasma. In order to simplify the qualitative analysis, we approximately think that T_e along the magnetic field line is the same.[27]

$$\phi = \phi_{CL} + T_e \log\left(\frac{n_0}{n_{CL}}\right). \tag{1}$$

It can be known from Eq. (1) that along the magnetic field line, the change of potential is mainly affected by the change of plasma density. As the plasma density on both sides of the thruster drops sharply, there is a decrease of the axial potential on both sides of the thruster. Because the magnetic pole attracts the negative charge and the effect of the sheath, the potential on the magnetic pole is lower. This potential difference will form an electric field towards the magnetic pole, and the acceleration of the ions by this electric field is the main reason for the bombardment of the ions to the magnetic pole.[27]

Meanwhile, through the comparison of the potential distribution in Fig. 6, it can be found that the potential distribution in the main beam area is not significantly affected by the additional electrode. But a closed potential contour pockets (PCPs) around the position of the additional electrode is created, and the potential can be enhanced near the additional location. This phenomenon is similar to the results in previous experiments and simulations.[28,29] Through the comparison of the three figures, it can be seen that the increase of the potential near the additional electrode is mainly in the range of $R = 0.046$ m–0.055 m. According to Eq. (1), the change of potential along the magnetic field line is mainly affected by the change of electron density along the magnetic field line, as this term $T_e \log(n_0/n_{CL})$. Under initial case, the potential in this area is low, mainly due to the relatively low electron density in this region. The electron density on the central axis is on the order of $10^{17}/m^3$, while the electron density near the upper boundary is one order of magnitude lower than that on the central axis. The additional electrode will attract electrons and increase the electron density near the additional electrode, thus reducing the difference of electron density between the upper boundary and the central axis and the value of this term $T_e \log(n_0/n_{CL})$. According to Eq. (1), the potential near the additional electrode will be increased. Since the potential near the main beam region is relatively high, the additional electrode has little effect on the parameters in the main beam region.

Since the change of potential will affect the ion movement, the effect of the additional electrode on the ion movement will be discussed later in this paper. Since the additional electrode mainly affects the upper region of the plume area, the effect of the additional electrode on the radial diffusion of ions and the bombardment on the outer magnetic pole by ions are mainly investigated.

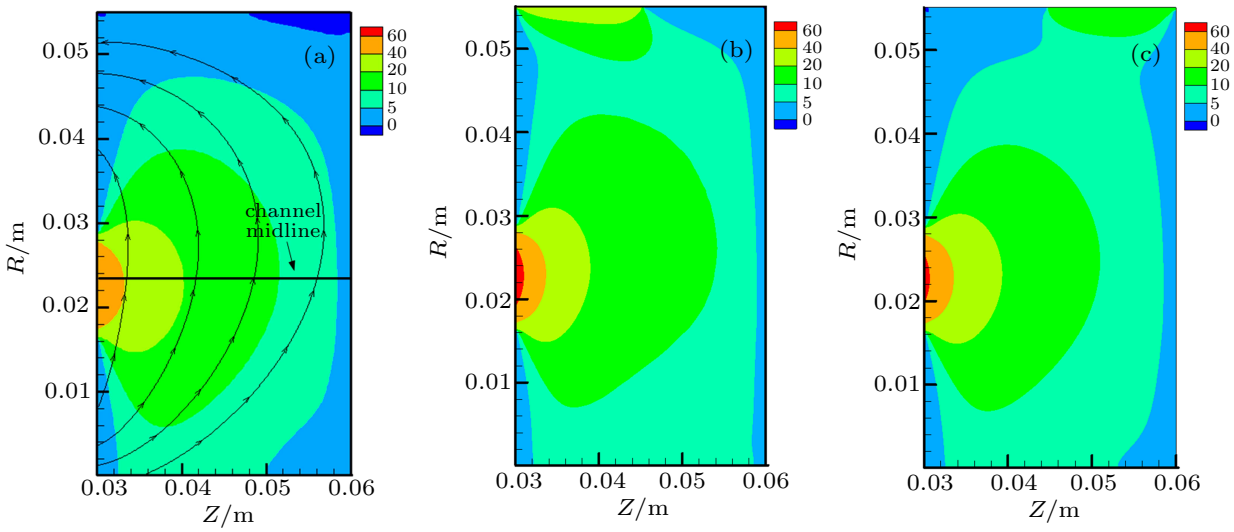


Fig. 6. The distribution of potential in the plume under the three conditions: (a) initial, (b) left 30 V, and (c) right 30 V.

3.2. Ion velocity distribution

In order to determine the influence of the additional electrode on the ion movement, we further compare the distribution of ion radial velocity at the upper boundary, as shown in Fig. 7. Through observation, it can be found that the additional electrode has a significant effect on the ion radial velocity, and the additional electrode can effectively suppress the radial acceleration of ions. As shown in Fig. 7, under initial case, the ion velocity at the upper boundary can reach 3800 m/s. Under the condition of the additional potential, the radial acceleration of ions can be effectively reduced. Under case-left 30 V, the radial velocity of ions near the additional potential can be reduced to within 1500 m/s, and the radial velocity of ions on the right side is also suppressed. As a result, the radial velocity of ions on the right side is also lower than that under the condition of initial. Under the condition of the additional electrode on the right side, the suppression effect of the additional electrode on the ions is more obvious, and the radial velocity of ions on the whole upper boundary region can be effectively suppressed.

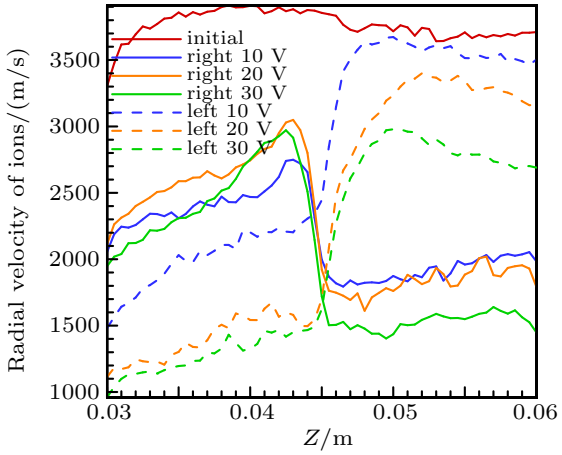


Fig. 7. The distribution of ion radial velocity at the upper boundary of the plume region under the seven conditions.

3.3. Ion flux distribution

In order to better illustrate the suppression effect of the additional electrode on the radial diffusion of ions, we further compared the differences in ion flux under seven conditions. Since the additional electrode has little effect on the main beam region, here we only compare the ion flux at the upper boundary of the plume region, as shown in Fig. 8. By comparison, it can be found that at the upper boundary position, the additional electrode can effectively reduce the ion flux. As shown in Fig. 8, in the region of $Z = 0.03$ m–0.045 m, the additional electrode can effectively reduce the ion flux under the condition of left electrode. Under case-left 30 V, the ion flux is relatively low, and the peak value of the ion flux can be reduced below $3 \times 10^{19}/(\mathrm{m}^2 \cdot \mathrm{s})$. According to the statistics of the total radial ion flux in this region, the total ion flux under case-left 30 V can be reduced by 81.32% compared with the condition of initial case. In the region of $Z = 0.045$ m–0.06 m, the additional electrode can also provide a good suppression effect on the ions under the condition of right electrode. Under case-right 30 V, the total ion flux can be reduced by 79.79% compared with the condition of initial case in this region. Through observation, it can be found that the area without the electrode is also affected by the additional electrode, and the ion flux is also reduced in varying degrees. According to the statistics of the total radial ion flux at the upper boundary ($R = 0.03$ m–0.06 m), the total ion flux under case-left 30 V and case-right 30 V is 57.7% and 59.8% lower than that under the condition of initial case. We also compared the effect of the additional electrode on the electron flux. The additional electrode has a significant attraction to the electron. The total electron flux near the additional electrode will be significantly increased. Under case-left 30 V and case-right 30 V, the total electron flux is 1.43 and 1.16 times higher than that under the condition of initial case. This is because the electron mass is relatively small and the additional electrode can provide more radial acceleration for the electron, so the radial flux has been significantly increased.

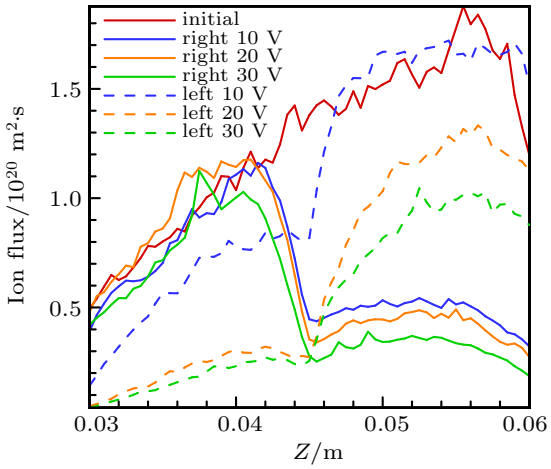


Fig. 8. Ion flux distribution at the upper boundary of plume region.

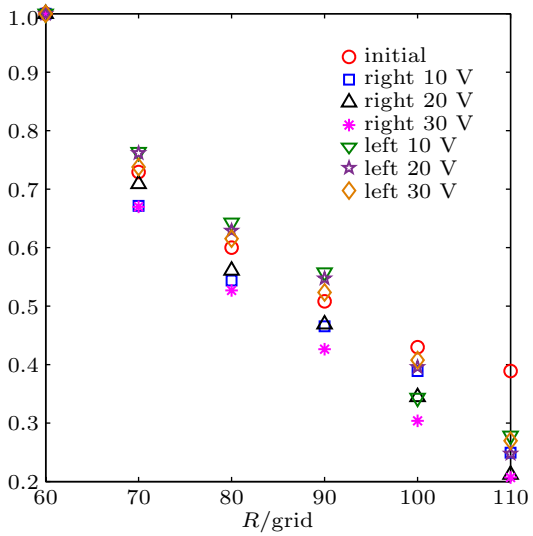


Fig. 9. The ratio of the total radial ion flux at different radial positions, based on the total radial ion flux at $R = 0.03$ m.

In order to determine the influence range of the additional electrode on the ion diffusion, we further compared the total radial flux of ions at different radial positions under these conditions. As shown in Fig. 9, we selected the radial position $R = 0.03$, 0.035, 0.04, 0.045, 0.05, 0.055 m. Then we make statistics of the total radial ion flux (the sum of the ion flux in the range of $Z = 0.03$ m–0.06 m) at each radial position, and normalize the total ion flux based on the total ion flux at $R = 0.03$ m. By comparison, we can find that at $R = 0.045$ m, there are some cases where the ion flux ratio is higher than that under the condition of initial. However, at $R = 0.05$ m the ion flux ratio under the condition of the additional electrode is all lower than the result under the condition of initial. Then at $R = 0.055$ m, this downward trend is more obvious. This shows that the influence range of the additional electrode on the radial diffusion of ions is between 0.045 m–0.055 m. The influence range of the additional electrode on the radial diffusion of ions is mainly affected by the potential distribution. As shown in Fig. 6, the influence range of the additional electrode on the potential is mainly $R = 0.046$ m $\sim$ 0.055 m, because the potential in this area is relatively low, the additional electrode can significantly improve the potential in this area. The increase of potential near the additional electrode will generate a radial electric field towards the main beam area, which will suppress the acceleration of ions in the radial direction. Therefore, the influence range of the additional electrode on the radial diffusion of ions is close to the region where the additional electrode affects the potential. The suppression of ion diffusion by the additional electrode is the main reason why the additional electric field reduces the plume divergence angle. The half plume divergence angle is also calculated under the seven conditions, as shown in Table 2. Under the condition of initial, the half plume divergence angle is 27.13°, which is close to the experimental results.[30] The calculation results are consistent with the analysis. And the existence of

the additional electric field can effectively reduce the plume divergence angle. Compared with the condition of initial, the plume divergence angle can be reduced by 18.2% under case-right 30 V.

Table 2. The half plume divergence angle under the seven conditions.

Condition	Initial	Right 10 V	Right 20 V	Right 30 V
Half plume divergence angle/(°)	27.13	24.2	23.27	22.19
Condition	Left 10 V	Left 20 V	Left 30 V	
Half plume divergence angle/(°)	26.8	25.9	25.5	

According to the previous analysis, the ions will not only diffuse towards the outside of the thruster, but also bombard towards the magnetic pole. Previous plume studies have shown that the change of the electric field in the plume area will have an effect on thruster magnetic pole erosion.[31,32] And ion bombardment on the magnetic poles is main reason for the erosion of the magnetic pole.[33–36] Since the additional electrode will affect the movement of ions, we further compare the ion flux on the outer magnetic pole, as shown in Fig. 10. It can be found by comparison that the existence of an additional electric field can enhance the ion bombardment on the magnetic pole. When the additional electrode is on the right side, the enhancement of ion bombardment on the magnetic pole is relatively small. However, when the additional electric field is on the left side, the ion bombardment on the magnetic pole is significantly enhanced, especially in the outer region of the magnetic pole. Under case-left 30 V, the peak value of ion flux on the magnetic pole can reach $1.025 \times 10^{20}/(\mathrm{m}^2 \cdot \mathrm{s})$. This phenomenon is similar to the phenomenon of serious pole erosion of the magnetically shielded thruster. The main reason for this phenomenon is due to the increase of the axial potential difference between the magnetic pole and the beam.[27,37–39] From the potential distribution in Fig. 6, it can be seen that the existence of the additional electrode enhances the potential of the nearby area and the accelerating electric field towards the magnetic pole, which leads to the enhancement of the ion bombardment on the magnetic pole. When the additional electrode is on the left side, the potential near the outer side of the magnetic pole increases more significantly, so the ion bombardment near the outer side of the magnetic pole is relatively serious. We further make statistics of the total ion deposition on the magnetic pole, as shown in Table 3. Through comparison, it can be found that under the condition of the left electrode, the total ion deposition on the magnetic pole is significantly increased, and it is doubled under case-left 30 V compared with the condition of initial. And under case-left 30 V, the total ion deposition on the outer magnetic pole accounts for 2.4% of the total ion flux of the thruster, so it can be considered that although the additional electrode will enhance the ion flux on the magnetic pole, the ion flux on the magnetic pole is still relatively low. In summary, the additional electrode on the left side can significantly enhance the ion bombardment on the magnetic pole. But the additional electrode is on the right side, the increase of ion flux on the magnetic pole is relatively small, which can avoid too much pole bombardment.

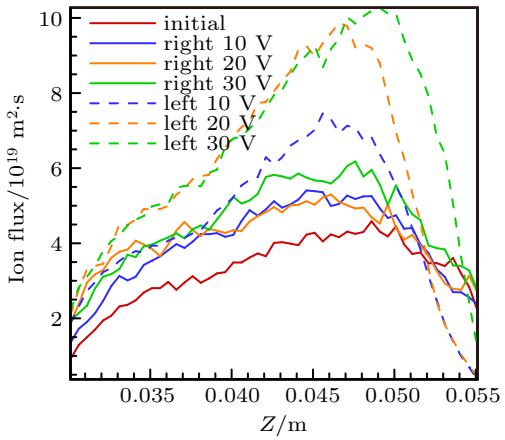


Fig. 10. Ion flux on the outer magnetic pole under the seven conditions. The range of outer magnetic pole is $Z = 0.029$ m–0.055 m.

Table 3. Statistics of total ion deposition on the outer magnetic pole.

Condition	Initial	Right 10 V	Right 20 V	Right 30 V
Total ion deposition/s	8.32×10^{17}	1.007×10^{18}	1.03×10^{18}	1.14×10^{18}
Condition	Left 10 V	Left 20 V	Left 30 V	
Total ion deposition/s	1.16×10^{18}	1.49×10^{18}	1.68×10^{18}	

4. Conclusion

This paper uses PIC-MCC simulation method to simulate and analyze the effect of additional electrode on the parameter distribution in the plume area of Hall thruster. The research results show that the existence of the additional electrode will significantly increase the potential near the location of the additional electrode, and the increase of the potential can effectively suppress the radial diffusion of ions. Comparing the plume divergence angle shows that the existence of the additional electrode can effectively reduce the plume divergence angle. When the additional electrode is 30 V, the half plume divergence angle can be reduced by 18.21%. But the existence of additional electrode will increase the ion flux on the outer magnetic pole, which will increase the erosion of the magnetic poles. The simulation results in this paper indicate that the ad-

ditional electrode is relatively outside, which not only can better reduce the plume divergence angle, but also will not cause excessive ion bombardment on the magnetic pole. Therefore, the following work can follow the design idea of additional electrode on the surface of the inner and outer poles to suppress the ion bombardment. The research work of this paper can provide a reference for the beam design of Hall thruster.

References

[1] Mazouffre S 2016 *Plasma Sources Sci. Technol.* **25** 033002
[2] Boeuf J P 2017 *J. Appl. Phys.* **121** 011101
[3] Kim H, Choe W, Lim Y, Lee S and Park S 2017 *Appl. Phys. Lett.* **110** 114101
[4] Goebel D M, Hofer R R, Mikellides I G, Katz I, Polk J E and Dotson B 2015 *IEEE Trans. Plasma Sci.* **43** 118
[5] Yuge S and Tahara H 2005 *The* 29*th International Electric Propulsion Conference*, October 31–November 4, 2005, Princeton, USA, IEPC-2005
[6] Linnell J A and Gallimore A D 2006 *Phys. Plasmas* **13** 103504
[7] Gabor D 1947 *Nature* **160** 89
[8] Morozov A I 2003 *Plasma Phys. Rep.* **29** 235
[9] Goncharov A A, Zatuagan A V and Protsenko I M 1993 *IEEE Trans. Plasma Sci.* **21** 578
[10] Goncharov A A, Dobrovolsky A, Protsenko I M, Kaluh V and Onishenko I 1998 *Rev. Sci. Instrum.* **69** 1135
[11] Granstedt E M, Raitses Y and Fisch N J 2008 *J. Appl. Phys.* **104** 103302
[12] Ahedo E and Parra F I 2005 *J. Appl. Phys.* **98** 023303
[13] Escobar D and Ahedo E 2008 *IEEE Trans. Plasma Sci.* **36** 2043
[14] Griswold M E, Raitses Y and Fisch N J 2014 *Plasma Sources Sci. Technol.* **23** 044005
[15] Liu H, Yu D R, Yan G J and Liu J Y 2008 *Contrib. Plasma Phys.* **48** 603
[16] Cao X F, Liu H, Jiang W J, Ning Z X, Li R and Yu D R 2018 *Chin. Phys. B* **27** 085204
[17] Liu H, Chen P B, Sun Q Q, Hu P, Meng Y C, Mao W and Yu D R 2016 *Acta Astronaut.* **126** 35
[18] Yu D, Li H, Wu Z and Mao W 2007 *Phys. Plasmas* **14** 064505
[19] Cao X F, Hang G R, Liu H, Meng Y C, Luo X M and Yu D R 2017 *Plasma Sci. Technol.* **19** 105501
[20] Li H, Xia G J, Mao W, Liu J W, Ding Y J, Yu D R and Wang X G 2018 *Chin. Phys. B* **27** 105209
[21] Liu H, Chen P B, Zhao Y J and Yu D R 2015 *Chin. Phys. B* **24** 085202
[22] Yu D R, Zhang F K, Liu H, Li H, Yan G J and Liu J Y 2008 *Phys. Plasmas* **15** 104501
[23] Mikellides I G, Katz I, Goebel D M, Jameson K K and Polk J E 2008 *J. Propul. Power* **24** 866
[24] Lev D, Alon G, Mykytchuk D, Alon G 2016 *The* 52*th AIAA/ASME/SAE/ASEE Joint Propulsion Conference*, July 25–27, 2016, Salt Lake City, USA, AIAA-2016-4732
[25] Goebel D M, Katz I 2008 *Fundamentals of electric propulsion: ion and Hall thrusters* (Chichester: John Wiley and Sons) p. 32
[26] Liu H 2009 *Study on characteristics of electron behaviours in hall thrusters*, Ph. D. dissertation (Harbin: Harbin Institute of Technology) (in Chinese)
[27] Ortega A L, Mikellides I G, Sekerak M J and Jorns B A 2019 *J. Appl. Phys.* **125** 033302
[28] Qing S W, E P, Xia G Q, Tang M C and Duan P 2014 *J. Appl. Phys.* **115** 033301
[29] Xu K G, Dao H and Walker M L R 2012 *Phys. Plasmas* **19** 103502
[30] Ding Y J, Su H B, Li H, Jia B Y, Wei L Q, Peng W J, Hu Y L, Mao Wand Yu D R 2019 *J. Vac. Sci. Technol. B* **37** 012902
[31] Kamhawi H, Huang W S and Mikellides I G 2018 *2018 Joint Propulsion Conference*, July 9–11, 2018, Cincinnati Ohio, USA, AIAA-2018-4720
[32] Ding Y J, Wang L, Fan H T, Li H, Xu W F, Wei L Q, Li P and Yu D R 2019 *Phys. Plasmas* **26** 023520
[33] Mikellides I G and Ortega A L 2014 *The* 50*th AIAA/ASME/SAE/ASEE Joint Propulsion Conference*, July 28–30, 2014, Cleveland, USA, AIAA-2014-3897
[34] Goebel D M, Jorns B A, Hofer R R, Mikellides I G and Katz I 2014 *The* 50*th AIAA/ASME/SAE/ASEE Joint Propulsion Conference*, July 28–30, 2014, Cleveland, USA, AIAA-2014-3899
[35] Hofer R R, Cusson S E, Lobbia R B and Gallimore A D 2017 *The* 35*th International Electric Propulsion Conference*, October 8–12, 2017, Atlanta, USA, IEPC-2017-232
[36] Polk J, Lobbia R, Barriault A, Guerrero P, Mikellides I and Ortega A L 2017 *The* 35*th International Electric Propulsion Conference*, October 8–12, 2017, Atlanta, USA, IEPC-2017-407
[37] Ortega A I, Mikellides I G and Katz I 2015 *The* 34*th International Electric Propulsion Conference*, July 6–10, 2015, Kobe, Japan, IPEC-2015-249
[38] Hofer R R, Polk J E, Sekerak M J, Mikellides I G, Kamhawi H, Verhty T and Herman D 2016 *The* 52*th AIAA/ASME/SAE/ASEE Joint Propulsion Conference*, July 25–27, 2016, Salt Lake City, USA, AIAA-2016-4825
[39] Ortega A L and Mikellides I G 2018 2018 *Joint Propulsion Conference*, July 9–11, 2018, Cincinnati Ohio, USA, AIAA-2018-4647